Lithium and boron diffusivity and isotopic fractionation in hydrated rhyolitic melts

Roberta Spallanzani, Kenneth T. Koga, Sarah B. Cichy, Michael Wiedenbeck, Burkhard C. Schmidt, Marcus Oelze, Max Wilke

Contributions to Mineralogy and Petrology (2022) 177: 74
https://doi.org/10.1007/s00410-022-01937-2

ORIGINAL PAPER

Lithium and boron diffusivity and isotopic fractionation in hydrated rhyolitic melts

Roberta Spallanzani[1] · Kenneth T. Koga[2] · Sarah B. Cichy[1,3] · Michael Wiedenbeck[3] · Burkhard C. Schmidt[4] · Marcus Oelze[3,5] · Max Wilke[1]

Received: 24 February 2022 / Accepted: 4 July 2022 / Published online: 22 July 2022

Abstract

Lithium and boron are trace components of magmas, released during exsolution of a gas phase during volcanic activity. In this study, we determine the diffusivity and isotopic fractionation of Li and B in hydrous silicate melts. Two glasses were synthesized with the same rhyolitic composition (4.2 wt% water), having different Li and B contents; these were studied in diffusion-couple experiments that were performed using an internally heated pressure vessel, operated at 300 MPa in the temperature range 700–1250 °C for durations from 0 s to 24 h. From this we determined activation energies for Li and B diffusion of 57 ± 4 kJ/mol and 152 ± 15 kJ/mol with pre-exponential factors of 1.53×10^{-7} m^2/s and 3.80×10^{-8} m^2/s, respectively. Lithium isotopic fractionation during diffusion gave β values between 0.15 and 0.20, whereas B showed no clear isotopic fractionation. Our Li diffusivities and isotopic fractionation results differ somewhat from earlier published values, but overall confirm that Li diffusivity increases with water content. Our results on B diffusion show that similarly to Li, B mobility increases in the presence of water. By applying the Eyring relation, we confirm that B diffusivity is limited by viscous flow in silicate melts. Our results on Li and B diffusion present a new tool for understanding degassing-related processes, offering a potential geospeedometer to measure volcanic ascent rates.

Keywords Stable isotopes · Diffusion · Isotopic fractionation · Hydrated silicate melts

Introduction

Volatile components dissolved in silicate melts can significantly affect magmatic processes such as crystallization, fragmentation, and eruption (e.g., Gonnermann and Manga 2007; Edmonds and Wallace 2017). Such components tend to exsolve from the magma during ascent due to their general low solubilities at low pressure, close to the surface. The most abundant volatile components in magmas are H_2O, CO_2, and sulphur-bearing compounds, SO_2 and H_2S. Particularly H_2O and CO_2 are important components controlling magma ascent and degassing because they are responsible for the formation and growth of gas vesicles during magma ascent. Bubble nucleation and growth occur when decompression causes a drop of solubility of the volatile components in the melt phase. For this reason, e.g., the bubble number density of erupted material is proportional to the ascent rate (Toramaru 2006). A variety of techniques has been developed to quantify magmatic ascent rates using chemical transport signatures, mineralogical, or textural observations of the erupted materials (e.g., Rutherford 2008; Browne and Szramek 2015), including bubble size and distribution (bubble number density) or melt inclusions in volcanic minerals (Pappalardo et al. 2018). Each of these methods has limitations and still leaves a considerable uncertainty on estimates of the ascent rate, hence the need to establish

Communicated by Gordon Moore.

✉ Roberta Spallanzani
spallanzani@uni-potsdam.de

[1] Institut Für Geowissenschaften, Universität Potsdam, Potsdam, Germany

[2] CNRS, IRD, OPGC, Laboratoire Magmas Et Volcans, Université Clermont Auvergne, Clermont-Ferrand, France

[3] GFZ German Research Centre for Geosciences, Potsdam, Germany

[4] Department of Mineralogy, Georg-August-Universität Göttingen, Göttingen, Germany

[5] Federal Institute for Materials Research and Testing, Berlin, Germany

new tools to improve our understanding on magmatic ascent and degassing processes.

The nucleation and growth of vesicles are mainly controlled by exsolution of H_2O and CO_2, while minor and trace volatile species are preferentially trapped into the gas phase, without controlling the bubble growth dynamics. Rather, the evolution of the gas bubbles is determined by the behaviour of the major constituents. Therefore, the abundance and distribution of these minor components can be used for tracing ascent and degassing processes (e.g., Gonnermann and Manga 2007; Edmonds and Wallace 2017). Lithium and boron are minor fluid-mobile components in silicate melts (e.g., Brenan et al., 1998; Tomascak et al. 2016), present in all volcanic systems in varying abundances and isotopic compositions (Barth 1993; Marschall et al. 2017; Penniston-Dorland et al. 2017; Leeman and Sisson 2018). They both have similar concentrations in silicate melts that are positively correlated to H_2O concentration in natural glasses. Lithium and boron both have two stable isotopes in nature (^{7}Li and ^{6}Li, 92.4% and 7.6%; ^{11}B and ^{10}B, 80.2% and 19.8%; Pfennig et al. 1998). Li and B isotopes are subject to isotopic fractionation occurring during heterogenous reactions, such as melting, crystallization and degassing, which leave geochemical signatures allowing for reconstruction of such reactions (e.g Wunder et al. 2011; Romer et al. 2014; Xiang et al. 2020). Moreover, due to the large mass difference, they may be also kinetically fractionated, during diffusive transport. Thus, both Li-B content and isotopic signatures around fluid-bubbles provide a basis for developing a speedometer for ascent and degassing rates during volcanic processes.

The structure of silicate melts can be described as a partially to fully polymerized network of silicon/aluminium-network-forming tetrahedra, with interstitial sites accommodating larger network-modifier cations (Mysen and Richet 2018). The degree of polymerization strongly depends on the chemical composition of a given silicate melt, and it plays a key role in any transport process such as intra-melt diffusion or melt viscosity. Lithium is a small-radius alkali metal, which occupies the interstitial position in the silicate melt network (Ross et al. 2015). In recent decades, several studies have investigated Li diffusivity in dry systems. Jambon and Semet (1978) and Cunningham et al. (1983) reported similar results for Li mobility, where Li was found to diffuse significantly faster than other cations, such as Rb or K. It was also observed that the melt composition has a small effect on Li diffusivity; this effect has been attributed to its size and structural position in the silicate structure. Two other investigations focused on the diffusivity and isotopic behaviour of Li in basalt–rhyolite glass couples (Richter et al., 1999, 2003), giving the first results on diffusion-driven isotopic fractionation in silicate melts. ^{6}Li was confirmed to show circa 12% faster diffusion than ^{7}Li (Lesher and Spera 2015). A more recent study reported chemical diffusion in hydrous rhyolitic melts (Holycross et al. 2018), establishing a dependence of Li diffusivity on the H_2O content of the silicate melt. Holycross et al. (2018) were the first to report results of diffusion-couple experiments employing two hydrous melts with the same major composition but with initially different Li concentrations (intra-melt diffusion). During fluid exsolution, ^{7}Li partitions preferentially into the fluid phase relative to ^{6}Li (Wunder et al. 2011), leading to a decrease in the δ^7Li in the silicate melt. Thus, if Li diffuses out of melt into the fluid (i.e., bubble), a preferential incorporation of ^{7}Li is expected during exsolution at equilibrium conditions, while ^{6}Li is preferred when Li transport by diffusion to the fluid bubble is the limiting factor.

Boron is an atypical network former, preferentially bonding with oxygens either in trigonal or tetrahedral coordination (Dell et al. 1983; Angeli et al. 2010; Bista et al. 2016). The coordination of B in silicate melts has significant effects on the physical properties of the host magma, influencing both viscosity and density (Dingwell et al. 2002). Several studies have been conducted on B speciation in a variety of glasses and melts. Generally, B is found in both trigonal and tetrahedral coordination. The heavier isotope is preferentially fractionated into the lower coordination number polyhedron (e.g., Kakihana et al. 1977). Hence, the heavy and most abundant isotope (80.2%) has stronger bonds with the silicate melt network than does the light isotope, with natural abundance of 19.8% (Pfennig et al. 1998). Schmidt et al. (2004) used NMR and Raman spectroscopy on dry, hydrous albite glasses with varying B concentrations. They determined that B in coordination [4] represents 2 and 6% of total for dry and hydrous conditions, respectively (with H_2O 4.4 wt%). However, B speciation is tightly controlled by the composition of the melt, particularly by the relative proportion of Si and Al: generally, an increase in the Si/(B + Al) ratio produces an increase in the [4] coordination of B (Lee and Lee 2020). Hervig et al. (2002) investigated the elemental and isotopic fractionation of B between a fluid phase and an associated silicate melt. They found fluid-melt element partition coefficients are < 1 for basaltic and > 1 for rhyolitic melts. Furthermore, they established that ^{11}B is preferentially fractionated into the fluid phase as compared to ^{10}B even at magmatic temperatures. Hervig et al. (2002) proposed that this strong fractionation is related to the difference in coordination between the melt and the fluid phase, i.e., ^{11}B is preferentially incorporated into the fluid phase with trigonal coordination, whereas ^{10}B is preferentially tetrahedrally coordinated, hence fractionated into silicate melts.

Despite the fact that three studies have already reported B diffusion coefficients in silicate melts, almost no data are available for B mobility in hydrous melts (Baker 1991;

Chakraborty et al. 1993; Mungall et al. 1999). Baker (1991) focused on B diffusion in dry melts of dacitic and rhyolitic composition with experiments at 1 GPa between 1300 and 1500 °C, while Chakraborty et al. (1993) investigated the interdiffusion of B and silicon between a silicate and a borosilicate glass, having B as major constituent, between 1200 and 1600 °C at 1 atm. They also measured the isotope ratio along the diffusion path of their samples, but no isotopic fractionation was detected. Mungall et al. (1999) studied B diffusion in haplogranitic melts, studying the effects of addition of sodium or water to the melt at 1 GPa and in the temperatures 1137–1600 °C. This is the only study that reports results for B mobility in hydrous silicate melts, showing that the presence of water increases the B diffusion rate.

Our study reports Li and B chemical diffusion and isotopic fractionation in hydrous rhyolitic melts at a pressure of 300 MPa, in the temperature range of 700–1250 °C. These data are necessary for using Li and B and their isotopes as potential tracers of dynamics in magmatic processes, such as fluid exsolution, magma mixing or differentiation, at the typical conditions down to a 10 km deep magma chamber (Huppert and Woods 2002; Zhang et al. 2010; Watson et al. 2017). Because Li and B are fractionated significantly during the exsolution of a gas phase, establishing a time-window is crucial where Li and B can be used to constrain the duration of, e.g., magmatic ascent and degassing. Hence, the established diffusivities and isotopic fractionation properties are the basis for potential geochemical tracers of magmatic degassing and related processes.

Methods

Experimental procedure

Natural obsidian from the well-studied Cerro de Los Posos volcano near Bandelier, New Mexico was used as a reference composition to produce a synthetic Fe-free glass with a rhyolitic composition (see Table 1). Components SiO_2, $CaCO_3$, Na_2CO_3, K_2CO_3, Al_2O_3, and MgO were mixed to produce the target composition. Using a simplified system that excluded iron and titanium oxides, we could prevent unwanted bubble formation during the experiments by suppressing crystallization of Fe-oxides, which serve as bubble nucleation sites (Hurwitz and Navon 1994). Two separate batches of glass were doped with different amounts of $Li_2B_4O_7$ that provided two starting glasses with different Li and B concentrations (Table 1), while maintaining identical isotopic ratios for both elements in the starting glasses of the subsequent diffusion-couple experiments.

The mixtures were placed in individual platinum crucibles and melted in a one-atmosphere oven at 1600 °C for 4 hours, quenched in a water bath (Cichy et al. 2011) and ground into fine powder. This procedure was repeated twice to get a complete homogenisation of the synthesized material. Afterwards, the obtained glasses were ground into powder with two grain sizes < 63 µm and 63–150 µm and then mixed in a 1:1 mass ratio (e.g., Cichy 2011), to reduce as much as possible the air-filled space between grains and to suppress bubble formation in the following steps of the experimental procedure.

Table 1 Composition of the synthetic glasses and the Los Posos rhyolitic obsidian

Oxide [wt%]	LPR_50	LPR_200	Los Posos rhyolite (Stanton 1990)
SiO_2	74.7 ± 0.5	74.6 ± 0.4	76.6
Al_2O_3	12.9 ± 0.2	13.0 ± 0.2	12.7
K_2O	3.76 ± 0.03	3.77 ± 0.03	4.60
Na_2O	3.92 ± 0.06	3.96 ± 0.04	4.10
CaO	0.35 ± 0.02	0.36 ± 0.02	0.31
MgO	0.04 ± 0.01	0.038 ± 0.005	0.02
Fe_2O_3	–	–	0.56
FeO	0.08 ± 0.03	0.07 ± 0.02	0.58
TiO_2	0.018 ± 0.03	0.03 ± 0.01	0.1
MnO	0.009 ± 0.003	0.009 ± 0.004	–
H_2O	4.2 ± 0.5	4.2 ± 0.6	
Lithium [µg/g]	58 ± 10	200 ± 10	35
Boron [µg/g]	180 ± 30	600 ± 30	–

To obtain bubble-free hydrous glass cylinders, a first synthesis at high pressure and temperature was performed using an internally heated pressure vessel (IHPV) present at the GFZ Helmholtz Zentrum in Potsdam. Platinum capsules 3 cm in length and 6 mm in inner diameter were filled with one endmember glass powder and distilled water to obtain a homogeneous glass with a water content of 4.2 wt%. To homogenise the water-bearing silicate melt, we performed IHPV experiments for 48 h at pressure and temperature conditions of 300 MPa and 1200 °C, with Argon as pressure medium. The quench was executed by shutting down the power of the heating unit, giving a cooling rate of ca. 5.2 °C/s down to 500 °C. The capsules were confirmed to have not leaked by comparing the weight before and after the experiment. Then the platinum capsule was peeled off leaving the glass intact. Approximately 5 mm thick slices were cut, mounted in epoxy, and polished before drilling multiple glass cylinders which had diameters of 3.6 mm. This procedure verified that the produced glass was bubble-free and homogeneous, before performing the diffusion-couple experiment. Subsequently, the polished surfaces of the two endmember glasses identical in major element composition but differing in Li and B contents, were put in contact within a platinum capsule. The bottom part of the capsule was flattened into a cylindrical shape to tightly fit

the glass cylinders, reducing the air trapped in the capsule after being sealed. All of our diffusion-couple experiments employed such capsules for a varying amount of time at different temperatures. Due to the presence of a chemical gradient, the conditions of pressure and temperature above the glass transition trigger the mobilization of Li and B between the enriched and the depleted endmembers. The process was then interrupted by a rapid quench, which rapidly stopped the diffusion process.

A set of ten diffusion-couple experiments was performed in an IHPV, using a sample holder prepared for rapid quench, which assured a cooling rate of ca. 150 °C/s (Berndt et al. 2002). Experiments DIFF1 to DIFF5 have been performed at the GFZ Helmholtz Zentrum in Potsdam (Germany), while DIFF6 to DIFF13 have been carried out at the Mineralogy department at the University of Göttingen (Germany). The pressure was kept constant at 300 MPa for all experiments, while temperatures and durations were varied from 700 to 1250 °C, and from 0 s to 24 h, respectively (see Table 2). The temperature was continuously controlled and registered by three S-type thermocouples (Pt–Rh) for the entire duration of the experiments. Afterwards, the quenched samples were sectioned lengthwise, and embedded in EpoFix cold set epoxy in a 25.4 mm diameter mould. Each of the three mounts was then polished to produce a flat sample with a < 1 µm surface roughness.

Analytical methods

A fully automated JEOL JXA-8200 electron probe microanalyser was used at the Institute of Geosciences of the University of Potsdam (Germany) to obtain chemical analyses of the end-product glasses. This electron microprobe is equipped with five wavelength-dispersive spectrometers. Analyses were operated with 15 kV accelerating voltage, 15 nA probe current, and a beam diameter of 5 µm. The analytical counting times were either 10 or 6 s for the element peak and 5 or 3 s for background positions. Analyses were standardized against glass calibrants obtained from the Smithsonian Institution, synthetic oxides, and Reference Materials purchased from Astimex Ltd.

The dissolved water content played a major role in this study. A potential water gradient between the two diffusion couples could cause unwanted effects on Li and B diffusion processes, because of their H_2O-dependent mobility. Thus, to be sure to pair homogeneous endmembers with similar water contents (maximum difference of 0.5 wt%), we performed line scans by micro-Raman spectroscopy across pieces of the starting glasses before the preparation of the diffusion-couple samples using a LabRAM HR 800 Raman spectrometer. Raman spectra were collected using a 532 nm laser and a grating with 300 lines/mm in the range 100–4000 cm^{-1} with a three-time data acquisition for 30 s. The water content was calculated following the procedure described in Behrens et al. (2006) and Schiavi et al. (2018) for rhyolitic glasses using the intensity of the OH-bands between 3000 and 3800 cm^{-1}. Subsequently, we compared the results with the difference to 100% of the major element analyses by the electron probe of the glasses. The Raman values for a given samples scattered within ± 0.5 wt%, similar to the standard deviation of the electron microprobe analyses.

For the measurement of Li and B concentrations, two analytical techniques were used: laser ablation inductively couple plasma mass spectrometry (LA-ICP-MS) and secondary ion mass spectrometry (SIMS). In the end, this paper reports concentration profiles and isotopic ratios acquired by SIMS, while LA-ICP-MS measurements were used for a

Table 2 Experimental conditions and diffusion coefficients for the diffusion couples

Sample	T [°C]	Duration [s]*	Heating rate	D_{Li} [m^2/s]	β_{Li}	D_B [m^2/s]
DIFF1	700	0 (785)	50 °C/min	$1.23\times10^{-10}\pm8\times10^{-11}$	0.17 ± 0.02	–
DIFF2	700	1800 (785)	50 °C/min	$7.57\times10^{-11}\pm4\times10^{-11}$	0.18 ± 0.02	–
DIFF3	800	1800 (905)	50 °C/min	$3.50\times10^{-10}\pm5\times10^{-11}$	0.15 ± 0.02	–
DIFF5	1000	0 (1145)	50 °C/min	$8.67\times10^{-10}\pm2\times10^{-10}$	0.19 ± 0.04	–
DIFF10	1200	0 (2205)	30 °C/min	$1.44\times10^{-9}\pm5\times10^{-10}$	0.15 ± 0.02	–
DIFF13	1050	900 (1905)	30 °C/min	$9.46\times10^{-10}\pm2\times10^{-10}$	0.20 ± 0.02	–
DIFF6	1000	86,400 (–)	30 °C/min	–	–	$2.4\times10^{-14}\pm3\times10^{-15}$
DIFF7	1100	72,000 (–)	30 °C/min	–	–	$6.0\times10^{-14}\pm9\times10^{-15}$
DIFF8	1200	72,000 (–)	30 °C/min	–	–	$1.5\times10^{-13}\pm1\times10^{-14}$
DIFF12	1250	72,000 (–)	30 °C/min	–	–	$2.6\times10^{-13}\pm2\times10^{-14}$
Activation energy E_a [KJ/mol]				57 ± 4		152 ± 15
Pre-exponential factor D_0 [m^2/s]				1.53×10^{-07}		3.80×10^{-08}

*Numbers in brackets report the heating phase duration, starting from around 50 °C, until the target temperature (plus 5 s for the quench phase). We used the sum of the two values for the model

preliminary evaluation of the diffusion profiles before SIMS acquisitions, being a more precise, but also more time-consuming analytical technique. Laser ablation craters could potentially give problems to the SIMS data acquisition, therefore, two procedures have been adopted: for samples from DIFF1 to DIFF5 the analyses were done on the two different halves of the sample, while for the remaining samples, the mounts have been re-polished after LA-ICP-MS analyses, prior to SIMS sessions. Lithium and boron data collection by LA-ICP-MS was done at the GeoForschungsZentrum Potsdam (Germany), which verified the presence of diffusion profiles after the experiments. Measurements were conducted using the Analyte Excite 193 nm ArF* excimer-based laser ablation (LA) system (Teledyne Photon Machines, Bozeman, MT, USA), coupled to a quadrupole ICP-MS iCAP by Thermo Scientific. The LA-system was equipped with a HelEx II two-volume ablation cell (gas flow in I/min; chamber 0.7 I/min; cup 0.25 I/min). Helium was used as a carrier gas for aerosol transport from the sample surface to the ICP ion source, having been mixed downstream with Ar as a make-up gas before entering the plasma. Operational parameters of the ICP-MS instrument and LA-unit were tuned for maximum sensitivity, low oxide formation based on the $^{232}Th^{16}O/^{232}Th$ ratio and low laser-induced elemental fractionation based on the $^{238}U/^{232}Th$ ratio using NIST SRM 610 (Jochum et al. 2011). We used ^{29}Si as internal standard and the certified reference material NIST610 for calibration of all elements.

Samples were ablated with line measurements parallel to the glass interface, of approximately 250 µm of length and 20 µm wide. Each such profile lasted for 30 s with a repetition rate of 10 Hz and an energy density of 2–3 J/cm^2 (see Supplementary materials Fig. S-1 for pictures LA-ICP-MS and SIMS analyses). The data reduction was done using the Iolite™ software (Paton et al. 2011) and the reduction scheme X_trace_elements_IS (Woodhead et al. 2007); we selected by visually inspecting the time intervals of the signal used for concentration analysis, which corresponds to the maximum raw signal. Uncertainty estimates for the element's concentrations were based on repeated measurement of the reference materials NIST612 and BHVO-2 g and are in general better than ± 10% (95% c.l.). For the lower temperature diffusion-couple experiments, LA-profiles approximately 700 µm in length were obtained across the interface of the diffusion couple, with a distance interval of 25 µm. For higher temperature experiments, we measured the Li and B concentrations along the entire length of the capsule, with distance of 150 µm between two points of analysis.

For precise analyses of Li and B abundances, as well as their isotopic ratios, we determined point profiles using the Cameca 1280-HR SIMS in Potsdam. A total of four SIMS sessions were conducted as part of our study: the exact analytical settings varied slightly between sessions, (see Supplementary materials for details). Prior to analyses, each mount was ultrasonically cleaned in high-purity ethanol prior to argon sputter coating that deposited a 35 nm thick, high-purity gold coating that was needed to assure electrical conductivity. All four analytical protocols used a $^{16}O^-$ primary beam operated in Gaussian mode, with a total impact energy of 23 keV, with 18 cycles per measurement. Absolute abundance values were calibrated using the two endmember synthetic glasses used in our experiments, which served as the calibration materials; these were assigned values for Li (58 and 200 µg/g) and B (180 and 600 µg/g) previously determined by LA-ICP-MS. Li and B concentration values were calculated by normalizing Li and B signals to the $^{28}Si^{++}$ mass signal at each point of analysis, to correct any possible mass effect from the SIMS analytical procedure. Isotopic ratios were not corrected for the instrumental mass fractionation, rather they are reported as delta notation referenced to the starting glass compositions.

To improve the analytical precision, multi-collection mode was applied to Li isotope measurements on two samples DIFF1–DIFF2. This modified approach was able to decrease the analytical uncertainty from ± 1.2 to ± 0.7% (1SE) as compared to mono-collection mode. A disadvantage of the static multi-collection approach is that concentration data cannot be obtained as the maximum dispersion of the 1280-HR does not allow for the acquisition of a major element reference mass (e.g., $^{28}Si^{++}$).

The relative variation of the isotopic ratio is expressed as δ^7Li and $\delta^{11}B$, normalized to a reference material (hydrated starting glasses of the two Li and B contents). Delta-notation were calculated by the following equation, where R_A is the atomic ratio of the isotopes of an element A (e.g., Hoefs 2009) of an unknown sample, related to a reference value:

$$\delta_A = \left[\left(\left(R_A\right)_{sample}/\left(R_A\right)_{ref}\right) - 1\right] \cdot 1000\%. \quad (1)$$

In this study, we decided to report a relative δ value, related to the reference material we used to calibrate the SIMS for Li and B concentrations and isotopic ratios. Therefore, the δ^7Li and $\delta^{11}B$ were calculated based on $(R_A)_{ref}$ defined by the bubble-free starting glasses used in our experiments. The measurements made on these two pieces served also as a verification that the two endmembers had the same isotopic ratio. The δ^7Li calculation was normalized with a $^7Li/^6Li$ ratio of 12.087 and $\delta^{11}B$ with a $^{11}B/^{10}B$ ratio of 3.900. Possible matrix effects on the δ^7Li have been considered as negligible, since these are usually related to changes in the SiO_2 content and our samples are chemically homogeneous, while no evidence of matrix

effects are known for B elemental and isotopic analyses (De Hoog 2018; Denny et al. 2021).

Data processing and modelling

Diffusion coefficients (D) have been calculated using a solution of Fick's second law, for two semi-infinite diffusion couples (e.g., Crank 1975), in the following equation:

$$C(x,t) = C_2 + 0.5 \cdot (C_1 - C_2)(1 - erf(x/(2\sqrt{Dt}))), \quad (2)$$

where C_1 and C_2 are the initial concentrations of each side of the diffusion couple and t is the duration of the experiment. The larger the value for D the faster will be the motion of the given atomic species in the diffusing medium (Fig. 1a). Equation (2) was used to determine the diffusion coefficient of both B and Li. In the case of experiment DIFF13, the diffusion process reached the end of the capsule (see Fig. S-2, Supplementary materials). Therefore, Fick's law had to be solved in a different way, because the boundary conditions differed from the other samples (Eq. 3). In DIFF13 the diffusion process was still in its early stage, therefore, the concentration curve at the end of the capsule could be calculated by considering the following equation (Crank 1975):

$$C(x,t) = \frac{1}{2}(C_1 - C_2)\left(erf\left(\frac{h-x}{2\sqrt{Dt}}\right) + erf\left(\frac{h+x}{2\sqrt{Dt}}\right) + erf\left(\frac{h+2l-x}{2\sqrt{Dt}}\right) + erf\left(\frac{h-2l+x}{2\sqrt{Dt}}\right)\right) + C_2. \quad (3)$$

Here C_1 is the initial concentration of the low-Li endmember, l is the total length of the couple, and h is the length of the low-Li endmember (Crank 1975).

We investigated the temperature dependence of the diffusion using an Arrhenius equation:

$$D = D_0 \exp\frac{-E_a}{RT}. \quad (4)$$

In this equation, D is the diffusion coefficient, R is the ideal gas constant, and T is the temperature of the experiment, while D_0 and E_a are the pre-exponential factor and the activation energy, respectively.

Lithium data processing needed a further step because significant diffusion already occurred during the initial heating ramp due to high mobility of Li at any temperature between the glass transition and the run temperature, indicated by the concentration profile of the zero-time experiment. During the heating ramp, D is not constant and changes with varying temperature and time. To better describe the diffusion of Li in our experiments, we solved the equation for $\overline{Dt}$, a product of diffusivity and time (Shewmon 2016). $\overline{Dt}$ is solved with the time integrated diffusivity:

$$\overline{Dt} = \int_0^t D(\tau)d\tau, \quad (5)$$

in which the diffusion coefficient D is a function of time and integrated over the entire duration of the experiment (Table 2). Time-dependent diffusion coefficients are derived from the heating history of the experiment, in combination with a pre-exponential factor (D_0) and an activation energy (E_a) of diffusion from the Arrhenius relations:

$$D(\tau) = D_0 \exp\left(\frac{-E_a}{RT(\tau)}\right). \quad (6)$$

In Eq. 6, $T(\tau)$ is the heating history. In practice, $\overline{Dt}$ of all Li diffusion experiments are fitted simultaneously for the best E_a and D_0 minimizing the weighted sum of the squared residuals. It should be noted that this correction tends to affect higher temperature diffusion experiments

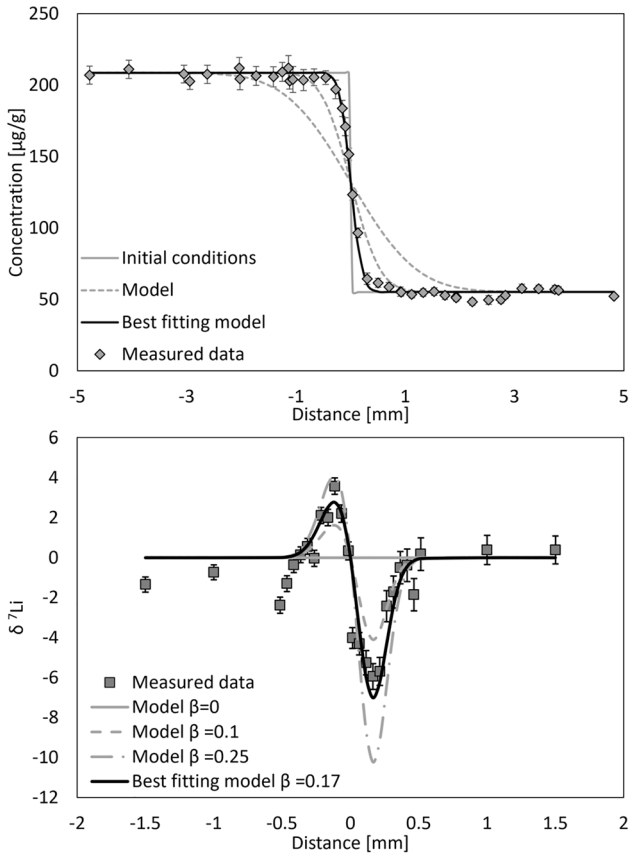

Fig. 1 Example of model fitting of concentration profile (**a**) and isotopic fractionation profile (**b**) for Li. The grey line in both plots represents the initial profile, while the dotted lines show intermediate profiles as a function of variable D, for the concentration profiles, and β for the isotopic fractionation model. The black line reports the best fit line

more towards lower diffusivity, for the same heating rate and duration.

Isotopic fractionation was modelled by calculating independently the diffusion coefficients for the concentration profiles of the two isotopes. By relating the two diffusion coefficients, we calculated the coefficient β (Richter et al. 2003), which defines the behaviour of the two isotopes in relation to each other, according to the equation:

$$\frac{D_{^7\mathrm{Li}}}{D_{^6\mathrm{Li}}} = \left(\frac{6}{7}\right)^{\beta}. \quad (7)$$

Using this approach, the profiles of two isotopes can be used for solving both diffusivity and β. The effect of β on the δ^7Li is shown in Fig. 1b, going from a value of 0, when there is no difference between the diffusivities of the two isotopes, to a value of 0.25, where the amplitude of the curve increases. The length of the profile affected by isotope fractionation is a function of the time during which the diffusion process is active.

All curve-fitting described above (Fig. 1a, b) was done by minimisation of the weighted sum of the squared residuals, in which the weights correspond to a reciprocal of squared uncertainty ($1/\sigma_{se}^2$). Furthermore, a Monte Carlo error propagation method was used to propagate the uncertainty of measurements to the final fit parameters. This is performed by repeating the curve fit and allowing a variation of concentrations with random sampling of a Gaussian distribution based on the observed experimental standard deviation (e.g., Anderson 1976) including the analyses of the major elements before and after the experiments. The small error given by the standard deviation demonstrates that the overall composition of the samples remains constant even after the experiments. The homogeneity of the samples has been verified by repeated measurements traversing from the core to the rims and the complete length of the glass cylinders.

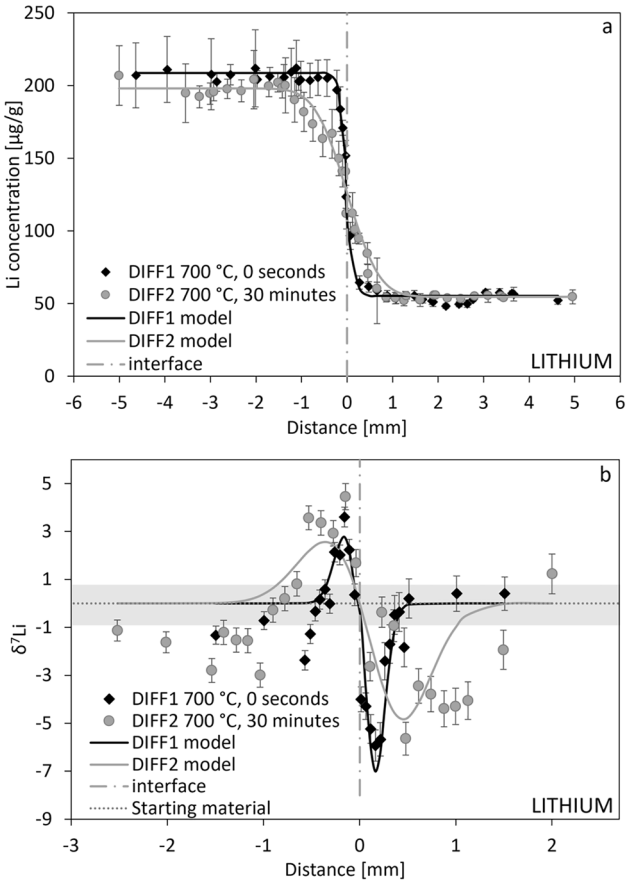

Fig. 2 **a** SIMS lithium concentration profiles of the samples DIFF1 and DIFF2, shown in black and grey, respectively. The dashed vertical line represents the original contact surface between the two glasses. The only difference between the two experiments is the duration, being 0 s for DIFF1 and 30 min for DIFF2. In 30 min, the diffusion had more time to proceed, resulting in a longer profile. **b** SIMS δ^7Li isotope profiles in multi-collection mode between the two experiments show that the wider sinusoidal shape is a result of the diffusion progression. However, the amplitude of the δ^7Li variation remain approximately the same in both profiles, as it only depends on the coefficient β. The grey area represents the uncertainty of δ^7Li of the starting material, which was analysed every five measurements, to verify the absence of analytical drift of the SIMS during the session

Results

Measurements of Li concentrations in two diffusion-couple experiments are shown in Fig. 2a (mono-collection SIMS results). The two experiments DIFF1 and DIFF2 were both performed at 700 °C for 0 s and 30 min, respectively. The length of the diffusion profiles reflects the different durations of the two experiments, where the longer profile is from the longer duration experiment. Significantly, DIFF1 shows that a diffusion profile is already present in an experiment that was immediately stopped after reaching the target temperature (zero-time experiment), indicating that the diffusion process started during the heating ramp, before reaching the final run-temperature (from 50 to 700 °C). Lithium diffusion not only is extremely fast (Richter et al. 2003; Holycross et al. 2018), but also starts at low temperature. Li diffusion was clearly identified and measured for binary Li_2O–SiO_2 glasses down to below 400 °C (Bauer et al. 2013). Taking this diffusion character into consideration, diffusion coefficients are determined and reported in Table 2, and the Li data yielded an activation energy of 57 ± 4 kJ/mol and a pre-exponential factor of 1.53×10^{-7} m^2/s (complete diffusion profiles of all samples are shown in Supplementary materials, S-3).

The diffusion-induced isotopic fractionation is shown in Fig. 2b, where the δ^7Li results of the SIMS multi-collection analyses of the samples DIFF1 and DIFF2 are shown. The significantly different mobilities of the two isotopes results

in a characteristic curve, which had also been reported by Richter et al. (2003) and Holycross et al. (2018). In this study we calculated β values in the range 0.15–0.20 (Table 2), following Eq. 7. The range of isotopic variation is constant regardless of the experimental parameters (Fig. 2b), because it is only controlled by the β coefficient. As it was the case for the concentration profiles, the length of the profile influenced by the diffusion, (i.e., starting from the contact surface of the two endmembers, the diffusion front is the area that is affected by particle migration, from the enriched to the depleted side of the diffusion-couple) changes with the duration of the experiment. The longer the experiment duration, the further the spread of the curve along the length of the capsule.

In contrast to the behaviour observed for Li, B is a significantly slower moving element. Figure 3a shows the results of two different diffusion-couple experiments, both at 1200 °C, with duration of 0 s and 24 h, respectively. In contrast with the case of Li, the length of the diffusion profile is visibly shorter, and the zero-time experiment produced no detectable diffusion in the sample. With this observation, we could ascertain that the heating ramp of the sample did not affect the diffusion of B. Overall, the results on B at all conditions resulted in an activation energy of 152 ± 15 kJ/mol and a pre-exponential factor of 3.80×10^{-8} for the Arrhenius relation (Table 2).

The isotopic results of B show profiles that are not as distinct as those for Li isotopes. In Fig. 3b, no clear trend is recognized and instead, the right-hand side shows a very slight decrease of δ^{11}B. Note that B diffusion flux was from left to right (from the high-concentration endmember on the left, to the low-concentration endmember on the right). In all the isotopic profiles of B, the low-B endmember results are systematically 1% lower than those of the high-B endmember.

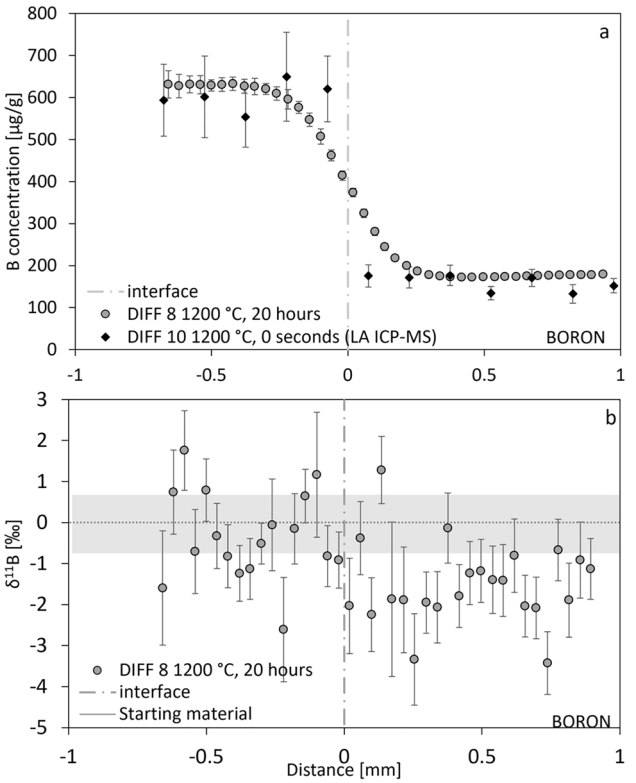

Fig. 3 **a** Boron concentration profile of two experiments, DIFF8 and DIFF10, with respective durations of 20 h and 0 s, both performed at a temperature of 1200 °C. SIMS measurements were not done for DIFF10. The results of Laser Ablation ICP-MS detected no diffusion, and, therefore, high-resolution SIMS analysis were considered unnecessary. **b** δ^{11}B isotope profile of the sample DIFF8 analysed by SIMS. The grey area represents the average value of the starting material, used as reference during the measurement sessions. There is a slight decrease in the δ^{11}B in the right part of the profile, corresponding to the low-concentration endmember

Discussion

Lithium and boron diffusivities

Figure 4a, b shows an Arrhenius diagram documenting the temperature dependence of the diffusion coefficients for Li and B as determined in this study. Clearly, Li is a significantly faster diffusing element than B. In the silicate composition used in this experiment, B acts as a network former, usually present in tetrahedral or trigonal coordination with oxygen (Angeli et al. 2010; Bista et al. 2016; Dell et al. 1983). Its bonds are similar to silicon in terms of strength; therefore, a large amount of energy is needed to first break bonds prior to commencing the diffusion process. Conversely, Li resides in the interstices of the silicate network, and hence diffusion can occur even at very low temperatures below the glass transition. In addition, water in silicate melts is a very efficient network modifier of the melt structure (Mysen and Richet 2018), facilitating the rupturing of oxygen bonds between network-forming ions, which leads to an increased mobility of both Li and B. In Fig. 4a, b it is apparent that the diffusivity studied here is higher than that measured in dry systems (Cunningham et al. 1983; Jambon and Semet 1978; Chakraborty 1993; Baker 1992).

Lithium

On the Arrhenius diagram (Fig. 4a) the data form a linear trend except for one outlier at 700 °C from experiment DIFF2. It is unclear why this experiment at 700 °C did not fit the overall pattern, as no irregularities were detected during experiment DIFF2. Generally, data at 700 °C have a higher uncertainty due to the stronger impact of the heating ramp on the overall diffusion profile. If the value of DIFF2 is an outlier, the activation energy for Li diffusion

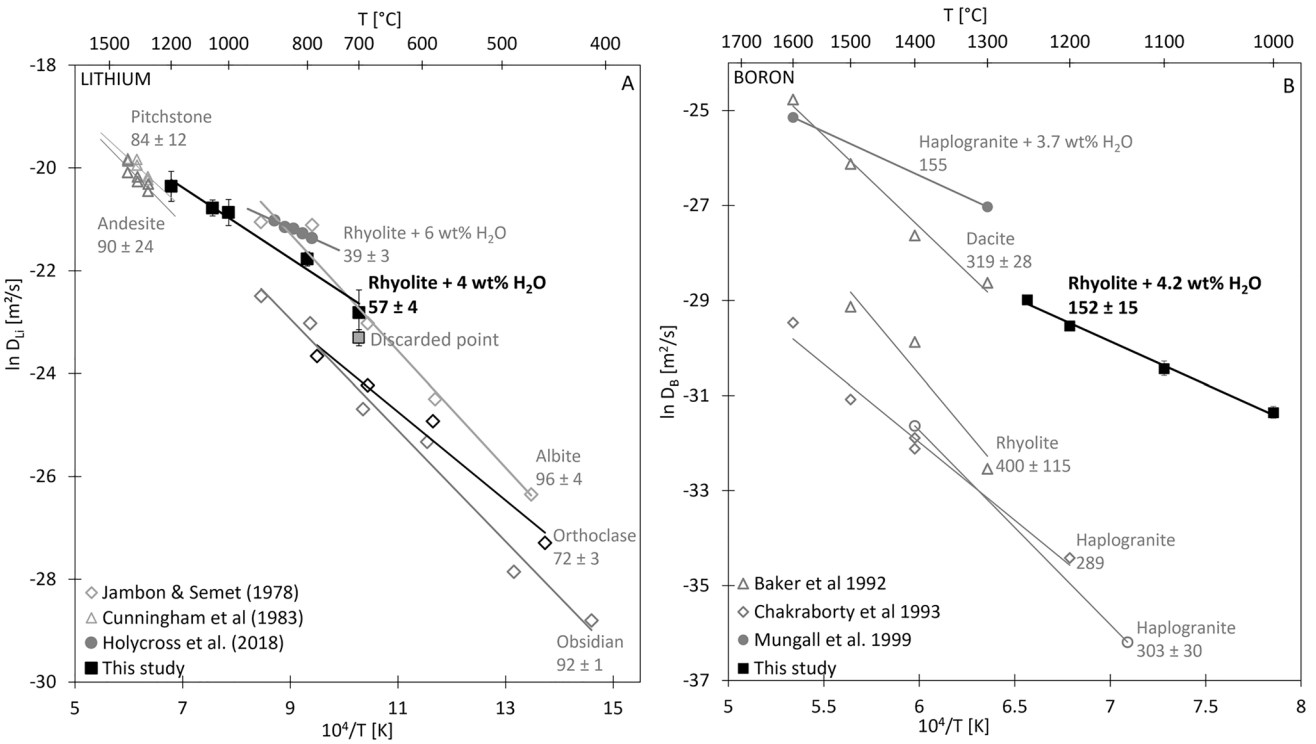

Fig. 4 Arrhenius relations of Li **a** and B **b** diffusivity of this study, compared to the available data on Li mobility in silicate melts. **a** All data reported with empty symbols are showing studies performed on dry silicate melts (Jambon and Semet 1978; Cunningham et al. 1983), while filled circles represent data from Holycross et al. (2018) investigating wet rhyolitic glasses with a H_2O content of 6 wt%. **b** Boron diffusivity data were compared with Baker (1992), Chakraborty et al. (1993), for dry systems, and Mungall et al. (1999) which reports B diffusion in hydrated conditions (H_2O 3.7 wt%). Activation energies reported for each dataset highlight that in hydrated silicate melts, the diffusion of Li and B is enhanced and proceeds faster than in the case of a dry matrix

in hydrous rhyolite is 57 ± 4 kJ/mol from linear regression, including the datum in the regression would yield an activation energy of 65 ± 6 kJ/mol. We concluded that 57 ± 4 kJ/mol is likely the true activation energy, since it is more coherent with the systematics compared with previous experiments, for example the relation of the activation energy to the water content, explained below.

In Fig. 4a our work is presented alongside the results of Cunningham et al. (1983), Jambon and Semet (1978), and Holycross et al. (2018). Of these three studies, the first two focused on anhydrous melts, while only Holycross et al. (2018) investigated Li diffusion in hydrous silicate melts. Our activation energy result is lower than the two anhydrous studies (90 ± 24 to 84 ± 12 and 72 ± 4 to 96 ± 3 kJ/mol from Cunningham et al. 1983 and Jambon and Semet 1978, respectively), suggesting that water presence in the silicate melt causes a decrease in the activation energy of Li. Our results are still higher than that reported for hydrous rhyolite, given by Holycross et al. (2018), which results in 39 ± 3 kJ/mol at 6 wt% H_2O. This difference is coherent with the expected effect of H_2O on the transport and is related to the change of melt structure with increasing H_2O. Therefore, the comparison of our results with different studies suggests that the activation energy of Li decreases linearly with the increase of the water content in the silicate melt as outlined in detail below.

Boron

Our diffusion results have been compared with the previous studies of Baker (1992), Mungall et al. (1999) and Chakraborty et al. (1993); these are plotted in an Arrhenius diagram in Fig. 4b. As compared to the result on hydrous melts reported by Mungall et al. (1999), our activation energy value differs only by 3%. Mungall et al. (1999) performed experiments at 1 GPa, while our experiments were conducted at 300 MPa. This may explain both the ca. one order of magnitude disparity between the absolute D-values and the significant difference in the pre-exponential factor of the Arrhenius fit (3.80×10^{-8} vs 2.51×10^{-7}). Despite this overall agreement, we note that Mungall's study only reports data obtained at two temperatures, and thus a comprehensive

evaluation on the differences between the two dataset is not possible.

Through the comparison with the studies of (Baker 1992 and Chakraborty et al. 1993), it is clear that B activation energy decreases strongly with increasing water content in a system, which is similar to the case for Li (Fig. 4b). Boron is a network former and coexists in silicate melts in either trigonal or tetrahedral coordination. The trigonal coordination is likely the dominant species in highly silicic melts, likely accommodating an extremely high percentage of the total B. Schmidt et al. (2004) verified that the presence of water enhances B [4] fold coordination species from 2 to 6% in metaluminous silicate melts. Nevertheless, we observed a significant decrease in the activation energy of B in the presence of water, meaning that the change in coordination of B is less important than is the decrease of the viscosity of the melt by water content (see below). These results have been compared with the study of Chakraborty et al. (1993), where B diffusion was investigated in a borate-silicate glass couple. That study shows strongly asymmetric profiles, related to the interdiffusion of B and silicon in opposite directions. Because boron was a major element in that study, the mass flux of B going in one direction has to be balanced by a silicon flux in the opposite direction. On contrast, concentration dependent diffusivity was not observed in our experiments (i.e., we did not find strongly asymmetric profiles), presumably because B is only a trace element: the trace quantities of B and Li were too insignificant to change the bulk melt structure. Furthermore, there was no interdiffusion of Si, as was the case for the study of Chakraborty et al. (1993), because in our experiments melt compositions of the diffusion couple were identical except for B (and Li).

Impact of water concentration

Water content has a major influence on both Li and B diffusion in silicate melts. Therefore, we investigated in more detail the water effect on their diffusivity, which mostly involves shifts in the activation energy. The main focus of this section is whether we can define a quantitative relationship between water content, melt composition, and Li and B mobilities.

Ross et al. (2015) investigated Li conductivity in aluminosilicate glasses. They stated in accordance with earlier studies (Kargl et al. 2006; Bauer et al. 2013) that Li diffusion is so fast because it is located in nano-sized low-dimensional domains, i.e., channels, that provide a percolation path within the structure of the silicate melt. At every jump of one cation to another site, an interstitial void with a negative charge potential is created and this is immediately occupied by another Li positive cation. This is likely facilitated if the melt is hydrated, as water is known to disrupt the tetrahedral network-connectivity of the glass (Le Losq et al. 2015). Further, there is evidence that H_2O is also arranged in low-dimensional units in silicate glasses as derived from X-ray diffratcion and Raman spectroscopy on natural rhyolite glasses (Zotov et al. 1992). This would also facilitate Li mobility.

Based on the available studies of the effect of melt composition on the Li diffusivity (e.g., Ross et al. 2015), we plotted the activation energy as a function of NBO/T, that represents the number of non-bridging oxygens per tetrahedral cation (Fig. 5a). This value was calculated following Mills et al. (2014) and it approximately describes the degree of polymerization of a glass. Water is well known to be a network modifier in silicate melts, generating non-bridging oxygens in the silicate structure, thereby increasing

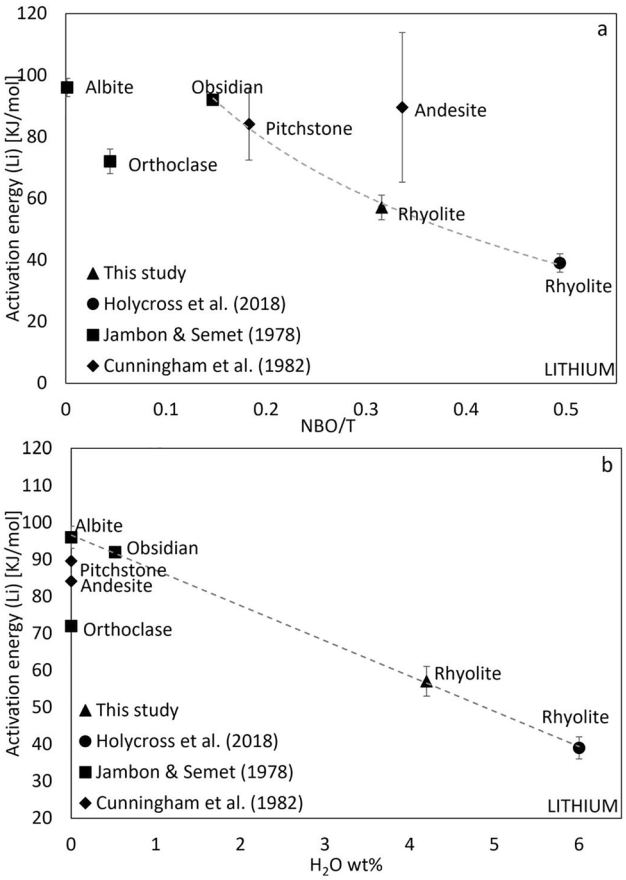

Fig. 5 **a** Activation energy of Li diffusivity as a function of the composition of the glass, with respect to NBO/T values. For comparable melt composition (rhyolite–obsidian–pitchstone) the activation energies decrease exponentially with an increase in the NBO/T value. For melts with significant compositional differences, there is a scatter in the dataset. **b** Activation energy of Li as a function of the water content of the studied glasses. For glasses with the same composition, the activation energy decreases linearly with the increase of water concentration. When the diffusivity of Li is studied in dry conditions, the major element composition of the glasses causes a scatter in the activation energy values

the NBO/T value (e.g., Mysen and Richet 2018). However, it has to be kept in mind that this value represents a simplified model that sorts cations according to simple rules. Furthermore, the ratio of molecular H_2O to OH-groups in silicate melts is temperature dependent, which is not accounted for in the calculation procedure (Stolper 1989).

In Fig. 5a, a scatter is seen in the available data from the various studies. Within the scatter, the obsidian of Jambon and Semet (1978), the pitchstone of Cunningham et al. (1983) and the two rhyolites by Holycross et al. (2018) and this study form an exponential trend. The activation energy decreases exponentially with increasing NBO/T, which is related to the water content. This trend appears to be valid only for melts with similar compositions. It is likely that the approach based on NBO/T does not adequately account for significant differences in major elements, as highlighted by the misalignment of the datapoints with strongly dissimilar chemical composition (albite, andesite, orthoclase).

As an alternative, we plotted the activation energy of Li against the water content (Fig. 5b). Figure 5b shows that the activation energy of Li diffusion correlates linearly to the water content of the melt. This property is particularly evident for the obsidian, the two rhyolites and the anhydrous albite glass. However, for those cases employing dry silicate melt, there is a spread of the datapoints with a significant variability in the reported activation energies. This is because even if Li is located in percolation pathways, as proposed by Ross et al. (2015), the bulk composition of the host medium nonetheless will play a significant role in Li diffusion, especially when no water is dissolved in the melt, particularly variations in the alkali-aluminum ratio may be important (Ross et al. 2015; Bauer et al. 2013). In addition, there could be some uncertainty related to the analytical precision of the major element measurements in the dry melts. Therefore, water contents have not been reported for all samples considered in comparison to our study, leading to possible uncertainties, though the observed scatter is too large to be explained solely by such an effect.

The diffusivity of B determined experimentally in this study was compared with values determined by the Eyring relation, using a viscosity calculated with the models described by Schulze, et al., (1996) and Giordano, et al. (2008). In the Eyring relationship it is assumed that the same transition state is passed during viscous flow and diffusion (Behrens and Haack 2007). The relation is shown in Eq. (8), where k_B is the Boltzmann constant, T is the temperature in K, η is the viscosity of the melt, and λ a characteristic jump distance for host medium:

$$D = \frac{k_B T}{\eta \lambda}. \quad (8)$$

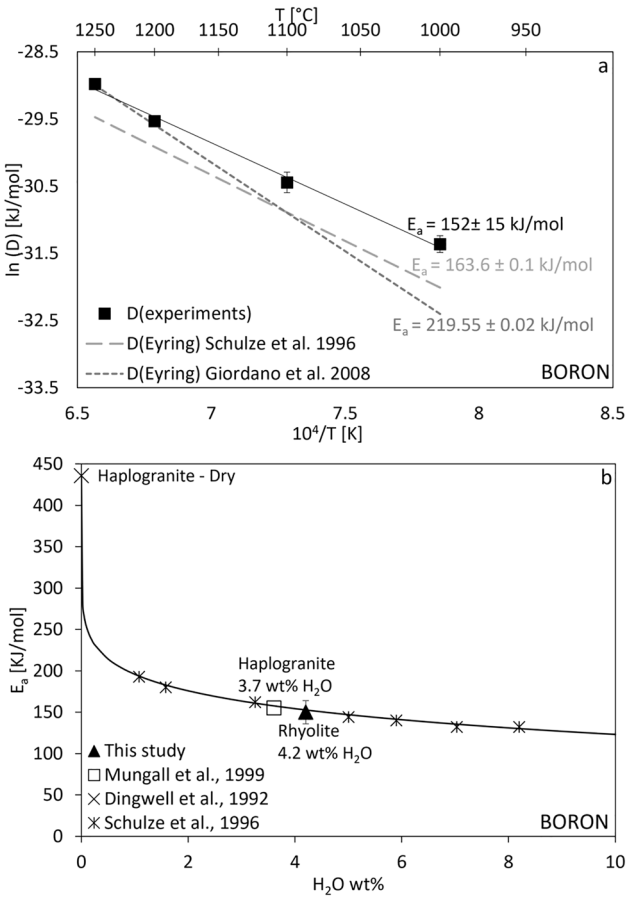

Fig. 6 **a** Arrhenius relation of the experimentally determined diffusion coefficients of B, and the empirical calculation of B diffusivity using the Eyring equation. The two different models use different viscosity estimations, by Giordano et al. (2008) and Schulze et al. (1996). The Arrhenius relation calculated using Giordano's viscosity is in better agreement with the experimental data for higher temperatures, but the slope of the trending line is steeper than the slope determined with our dataset, resulting in a significantly higher E_a (220 kJ/mol). The calculation made with Schulze's viscosity has a better agreement in the slope and determination of the E_a, (164 kJ/mol) with a shift in the entire dataset, due to the model parameters. **b** The overall agreement of the two models with the experimental data indicates that B diffusion is a process of viscous flow (Mungall 2001) and allows to compare E_a(B) with E_a from Schulze et al. (1996). The data from this study and from Mungall et al. (1999) show exceptional agreement with the plot from Schulze et al. (1996), therefore, we can numerically describe the effect of water on the mobility of B in highly silicic melts

The Eyring equation was successfully used to describe the diffusion of slow-moving ions such as Si and O (e.g., Chakraborty 1995; Mungall 2002), using a characteristic jump length of 0.3 nm. This value coincides with the diameter of the SiO_4-tetrahedron (Behrens and Haack 2007). Therefore, this relation provides a lower limit of diffusion for a given silicate melt composition and temperature, which is controlled by viscous flow. Figure 6a shows the Arrhenius relation of the three datasets, showing that overall our

experimental results are in good agreement with the two sets calculated from the viscosity models. The diffusivity obtained from the viscosity calculated according to Schulze et al. (1996) results in similar linear trend and similar activation energy (164 kJ/mol). We observe a small shift between the two datasets (difference ln $D = 0.5$), which might be attributed to the differences in the composition of the two glasses: haplogranitic in the case of Schulze et al. (1996) and rhyolitic for our study (Table 1). Using the viscosity calculated according to Giordano et al. (2008), the diffusivity data are in good agreement at high temperature (1200–1250 °C) but the model deviates with a steeper slope and consequently a higher activation energy at lower temperatures (Fig. 6a). The equation of Schulze et al. (1996) was calibrated using a set of hydrous haplogranitic samples, which were very close to our rhyolitic composition, while the model of Giordano et al. (2008) was calibrated using a wide spectrum of compositions. Nonetheless, the good agreement of our results with the Eyring equation allows us to consider B diffusion as primarily associated to the viscous flow dynamics (Mungall 2002), and thus we may use the activation energy determined for the viscosity and its relation to the water content of the silicate melt (Schulze et al. 1996) to extrapolate to B diffusivity. In Fig. 6b, we plotted the activation energy of B diffusivity determined by both our study and existing literature as a function of water content, and compared our diagram with the corresponding data of Schulze et al. (1996). The two datasets are in an exceptionally good agreement. The two points of our study and Mungall et al. (1999) related to measured diffusivities lie perfectly on the trend line defined by Schulze et al. (1996), confirming that B diffusion is limited by viscous flow and that the presence of water strongly affects the mobility of B, especially for water concents below 1 wt%, while for increasing water concentrations, the effects on B mobility is still significant, but less pronounced.

Isotope fractionation

Due to their mass difference, isotopes of an element diffuse at different rates in the same medium which is described by the coefficient β (e.g., Richter et al. 2003). Our evaluation of the diffusion-couple results determined the β values between 0.15 and 0.20 for Li but detected no significant isotope fractionation for B (i.e., incalculable β values). When Li diffuses from the high-Li segment, ^{6}Li moves faster than ^{7}Li, resulting initially in a more negative δ^{7}Li on the low-concentration segment and more positive (or heavier) δ^{7}Li on the high-concentration side of the interface (Fig. 2b). At the edges of the two endmembers, far away from the interface area, the isotope ratios remain undisturbed. Thus, the diffusive fractionation generates a characteristic curve for the isotope ratio across the interface, where β values can

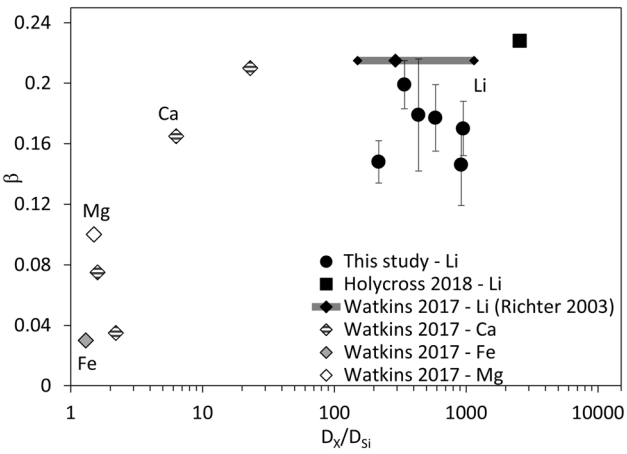

Fig. 7 β coefficient of an element X as a function of the diffusivity of the element, normalized to the diffusion coefficient of silicon (plot modified after Watkins et al. 2017; Holycross et al. 2018). The diffusivity of silicon for this study was calculated using the method of Baker and Bossányi (1994). For the study by Richter et al. (2003) Watkins took an average value of the diffusivity of silicon, as it migrates from higher to lower value, during the progress of diffusion between rhyolite and basalt. In this plot, we indicate the likely range for Si diffusivity, with the grey with diamond symbols both ends

be determined by fitting Eq. 7. In Fig. 7, we plotted the coefficient β as a function of the diffusivity of the element normalized to the diffusivity of silicon, to compare Li with several other cations, such as Ca, Mg, and Fe (Watkins et al. 2009, 2017; Holycross et al. 2018). D_{Si} was calculated following Baker and Bossányi (1994). Our β values are lower than those determined previously by Holycross et al. (2018), and Richter et al. (2003) but higher than was the case for many other elements.

It is generally considered that the more freely an element can migrate in a medium, the closer β approaches the value for an ideal gas of 0.5 (Richter et al. 2003). Because Li is a small cation which does not bond with the tetrahedral network, it is coherent to find that the obtained β values of all three studies (including ours) were higher than for other cations, even though the experiments used quite different designs. For example, the first report of β was determined by a diffusion-couple experiment with a natural rhyolite and a Li-doped natural basalt, performed under dry condition at 1.2–1.3 GPa, 1300–1350 °C (Richter 2003). That study reported $\beta = 0.215$, which is distinctly higher than our results (from 0.15 ± 0.02 to 0.20 ± 0.02). We suspect that the different experimental designs are the main cause of the disparity. Furthermore, in Richter et al. (2003) multi-component exchanges occur simultaneously with Li diffusion due to the basalt-rhyolite couple. Silicon is likely one of these diffusing species for a rhyolite-basalt couple, and, therefore, the value of D_{Li}/D_{Si} should have varied during the progress of diffusion. That means, the β value of Richter et al. (2003)

would have shifted from lower to higher values (Fig. 7). In our study, the diffusion couple is only driven by the chemical potential gradient of Li (i.e., both halves of the diffusion pair had the same matrix composition) reaching almost the condition of tracer or even self-diffusion. The study of Holycross et al. (2018) conducted similar experiments to ours and reported a β value of 0.228. A notable difference between the two experimental setups is the content of water dissolved in the silicate melt: 4.2 wt% for ours and 6 wt % for Holycross et al. (2018). While the differences between the isotope diffusivities is explained by differences of melt properties due to temperature and water content, we are not aware of any model relating the isotopic fractionation factor to melt properties. For example, our β values reveal no correlation with temperature. The discrepancy in the beta values seems likely be due to the difference in water content, suggesting that increasing water content facilitates the mobilization of ^{6}Li stronger than ^{7}Li, causing a greater effect on the isotopic ratio (Fig. 7).

The boron isotope data from our experiments show a different scenario compared to Li. No specific trend in the isotopic ratio was detected (Fig. 3b). Instead, a slight decrease in the isotopic ratio is observed on the side with lower B content in three of the four experiments (see isotopes profiles, Appendix). Possible effects related to irregularities in the starting glasses or in the sample analyses were excluded, as repeated measurements of the two reference materials were made every five measurements of the samples (both SIMS and LA-ICP-MS). Furthermore, no matrix or drift effects of the measuring instruments were recognized, and it was verified that the two endmembers had uniform isotopic ratio before the experiments. Lastly, this slight decrease in B isotopic ratio was observed only for experiments in which diffusion had occurred. In zero-time experiments, the isotopic ratio remained constant throughout the entire profile.

Boron isotope results are very difficult to interpret, possibly because of the more complex structural incorporation of B in the silicate melt. The observed variation in the isotopic ratio across the profiles might be generated by a combined effect of diffusive isotope fractionation and equilibrium isotope fractionation between trigonal B and tetrahedral B, rather than a lack of diffusive fractionation. It was shown that the difference in diffusivity of trigonal and tetrahedral B explains the concentration dependent diffusivity (Chakraborty et al. 1993) and trigonal B diffuses faster in the melt. Equilibrium isotope fractionation between trigonal and tetrahedral B favours heavy B (i.e., ^{11}B) in trigonal coordination. Combining all this for the B diffusion experiments: the faster moving trigonally coordinated B has heavier isotopic composition. Yet, due to diffusive fractionation, the lighter trigonal species potentially moves faster than the heavier one. Considering that tetrahedral B for albite melts has been estimated around 6% in hydrous conditions (Schmidt et al., 2004), our isotope profiles might result from the cancellation of the isotopic signature across the diffusive interface, combining the faster moving trigonal B (mostly ^{11}B) with normal diffusive fractionation favouring the light isotope migration. Thus, the data from this study do not show a distinct isotope fractionation. Quantitative modelling of such a complex scenario is not presented here as there are too many unconstrained parameters, but this clearly warrants future attention.

Lack of boron isotopic fractionation was previously discussed by Chakraborty et al (1993). The isotopic profile presented in Fig. 3b does show a change in the isotopic ratio of B isotopes; however, this change is too small to allow a clear calculation of a β coefficient. One possible explanation is that at the conditions of the experiments performed, the two isotopes have a slightly different behaviour, which is too small to generate a significant isotopic fractionation. Alternatively, isotopic fractionation might have a different time window compared to the diffusion rates of elemental B. The experiments performed during this study may have been too short if the isotopic fractionation takes place at lower rates than the elemental diffusion. In this case, the isotopic fractionation is hardly visible because the fractionation effects were too small to be detected. As all our runs do not show significant isotopic fractionation, we conclude that the effect of isotopic fractionation during B diffusion is small and undetectable at the experimental parameters used during this study. Finally, it should be noted that the absence of a detectable isotopic fractionation may result of the analytical technique employed. Here, the spatial resolution may not have been not good enough to correctly capture the effects of B isotopic fractionation. Different techniques, which allow smaller analytical spots and smaller distance between spots can clarify a potential effect, and might help establishing a value for the β coefficient of B.

Summary and future applications to volcanic systems

Lithium and B are fluid-mobile components in magmas stored at depth, and they passively participate in the dynamics of bubble nucleation and growth, which may trigger and define the volcanic eruption style. In this study, diffusion-couple experiments were performed to better constrain self-diffusion of Li and B in hydrous silicate melts. From the evaluation of the results, we confirmed that Li and B diffusivity are significantly influenced by the concentration of water in the system.

Lithium diffusion is extremely fast and starts at temperatures well below 700 °C. Its diffusivity is directly proportional to the concentration of H_2O in the silicate melt,

(Fig. 5b) while Li isotopic fractionation seems to be affected additionally by the major element composition of the silicate melt. The coefficient β calculated by the model fitting is slightly lower than what has been previously published; the observed differences are likely due to very different experimental setup (Richter et al. 2003) or the different water content (Holycross et al. 2018).

Boron diffusion occurs at slower rates as compared to Li. When it is a major constituent of the glass composition, B is strongly influenced by silicon interdiffusion, as the mass flux of the diffusion reaction needs to be maintained in both directions (Chakraborty et al. 1993). When B is present as a trace element the diffusion of silicon in the opposite direction can be neglected. Even though the presence of water enhances the amount of tetrahedrally coordinated B species, the effect on the structural position of B is negligible compared to the impact of the decrease in viscosity by dissolved H_2O in the silicate melt, which facilitates B diffusion in a very similar manner as viscous flow.

The very slight changes in the isotopic ratio of B isotopes seem to address to a diffusion-induced isotopic fractionation. Several scenarios have been proposed to explain the results shown in this study, but no clear explanation of the observation could be made. Further investigations will be required to get a complete picture of the dynamics of this process. Based on the timescale of the diffusion process, we believe that B isotopes could still be useful to record degassing phenomena and slow-moving fluid migration inside a magma chamber despite no clear isotopic signature was recognised in our data.

With the information from this study, we were able to estimate timescales of lithium and boron diffusion in hydrous or dry rhyolitic melts to estimate their applicability as a speedometer for ascending and degassing magmas. For this estimate, we used the model of Toramaru (2006), which relates the size and distribution of gas bubbles in melts to the decompression rate of a magma. Assuming a temperature of 1000 °C, we can estimate the average distance between bubbles in a magma ascending at different decompression rates (from 10 MPa/s to 0.001 MPa/s). The obtained distances range between 0.08 and 0.7 mm. Knowing the diffusion coefficient of Li and B from this study, we could calculate an approximate homogenisation time for the two elements and for the different decompression rates (see Fig. 8). The homogenisation time can be considered as the maximum time where any diffusion profiles may be retained and modelled. Having significantly different diffusion coefficients, Li and B can be combined to observe a wider range of process timescales: from seconds to hours for Li, and from hours to weeks or months for B. These estimated timescales highlight the potential use of Li and B as a speedometer for volcanic ascent rates. It has to be further considered, that melt-gas phase separation produces

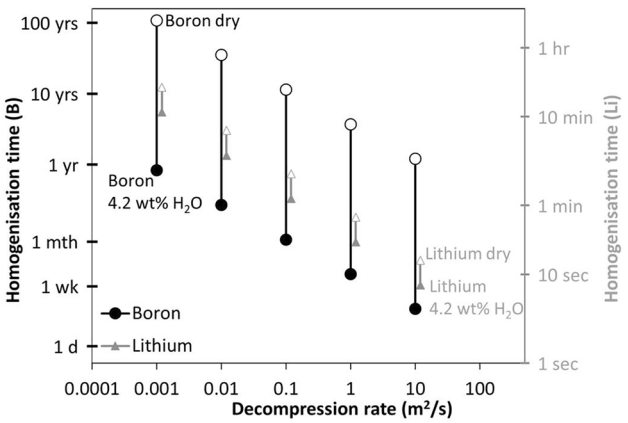

Fig. 8 Homogenisation times of Li (grey triangles) and B (black dots) for different decompression rates of a magma at 1000 °C and with a water concentration of 4.2 wt% (full symbols) or in dry conditions. These points represent an approximate time that the system needs in order for the diffusion of Li and B to lead to complete homogenization during magmatic degassing

changes in the isotopic ratio of volatile components (Watson 2017), which may be superimposed on the signature produced by diffusion-induced isotopic fractionation. Thus, decompression experiments performed at different decompression rates are needed to provide information about how Li and B behave during volatile exsolution and how isotopic fractionation evolves during bubble nucleation and growth. In any case, the ability to associate decompression rates (and thus, magma ascent rates) with the chemical and isotopic distribution of Li and B between growing bubbles and melt, would lead to the development of a precise speedometer applicable to erupted products of highly silicic volcanoes, so that Li and B will serve as an additional tool for tracing magmatic ascent and degassing rates prior to volcanic eruptions.

Supplementary Information The online version contains supplementary material available at https://doi.org/10.1007/s00410-022-01937-2.

Acknowledgements We thank Christine Fischer and Jens Bölke for their support in all the practical steps of sample preparation, and for the support in mechanical and technical issues encountered during this project. We would like to thank also the entire mechanical workshop of the GFZ, particularly Reik Sünkel, Michael Voigt and Michael Kreplin for their precious support for the management of the experimental setup. We are also grateful to Christina Günther for the essential help for EPMA analyses, Uwe Dittman for SIMS sample preparation and Frédéric Couffignal for the analytical contribution during all SIMS sessions. We also acknowledge the Deutsche Forschungsgemeinschaft for financial support through the project WI 2000/14-1.

Funding Open Access funding enabled and organized by Projekt DEAL.

References

Anderson G (1976) Error propagation by the monte carlo method in geochemical calculations. Geochim Cosmochim Acta 40(12):1533–1538. https://doi.org/10.1016/0016-7037(76)90092-2

Angeli F, Charpentier T, De Ligny D, Cailleteau C (2010) Boron speciation in soda-lime borosilicate glasses containing zirconium. J Am Ceram Soc 93(9):2693–2704. https://doi.org/10.1111/j.1551-2916.2010.03771.x

Baker DR (1991) Interdiffusion of Hydrous dacitic and rhyolitic melts and the efficacy of rhyolite contamination of dacitic enclaves. Contrib Miner Pet 106(4):462–473. https://doi.org/10.1007/BF00321988

Baker DR (1992) Tracer diffusion of network formers and multicomponent diffusion in dacitic and rhyolitic melts. Geochim Cosmochim Acta 56:617–631. https://doi.org/10.1016/0016-7037(92)90086-X

Baker DR, Bossányi H (1994) The combined effect of F and H2O on interdiffusion between peralkaline dacitic and rhyolitic melts. Contrib Miner and Pet 117:203–214. https://doi.org/10.1007/BF00286843

Barth S (1993) Boron isotope variations in nature: a synthesis. Geol Runds 82:640–651. https://doi.org/10.1007/BF00191491

Bauer U, Welsch AM, Behrens H, Rahn J, Schmidt H, Horn I (2013) Li diffusion and the effect of local structure on Li mobility in Li_2O–SiO_2 glasses. J Phys Chem B 117:15184–15195. https://doi.org/10.1021/jp408805e

Behrens H, Haack M (2007) Cation diffusion in soda-lime-silicate glass melts. J Non-Cryst Solids 353(52–54):4743–4752. https://doi.org/10.1016/j.jnoncrysol.2007.05.178

Behrens H, Roux J, Neuville Daniel R, Siemann M (2006) Quantification of dissolved H2O in silicate glasses using confocal Micro-Raman spectroscopy. Chem Geol 229:96–112. https://doi.org/10.1016/j.chemgeo.2006.01.014

Berndt J, Liebske C, Holtz F, Freise M, Nowak M, Ziegenbein D, Koepke J (2002) A combined rapid-quench and H2-membrane setup for internally heated pressure vessels: description and application for water solubility in basaltic melts. Amer Miner 87:1717–1726. https://doi.org/10.2138/am-2002-11-1222

Bista S, Morin EI, Stebbins JF (2016) Response of complex networks to compression: Ca, La and Y aluminosilicate glasses formed from liquids at 3 GPa pressures. J Chem Phys 144:044502. https://doi.org/10.1063/1.4940691

Brenan JM, Ryerson FJ, Shaw HF (1998) The role of aqueous fluids in the slab-mantle transfer of boron, beryllium, and lithium during subduction: experiments and methods. Geochim Cosmochim Acta 62(19/20):3337–3347. https://doi.org/10.1016/S0016-7037(98)00224-5

Browne B, Szramek L (2015) Rates of magma ascent and storage. In: Sigurdsson H (ed) The encyclopedia of volcanoes, 2nd edn. Academic press: Elsevier, Amsterdam, pp 203–214. https://doi.org/10.1016/B978-0-12-385938-9.00009-2

Chakraborty S (1995) Diffusion in silicate melts. In: Stebbins JF, McMillan PF, Dingwell DB (eds) Structure, dynamics, and properties of silicate melts. De Gruyter, Berlin, Boston, pp 411–504. https://doi.org/10.1515/9781501509384-012

Chakraborty S, Dingwell DD, Chaussidon M (1993) Chemical diffusivity of boron in melts of haplogranitic composition. Geochim Cosmochim Acta 57:1741–1751. https://doi.org/10.1016/0016-7037(93)90110-I

Cichy SB. (2011) Experimental study on vesiculation and formation of groundmass microlites induced by decompression: constraints on processes related to magma ascent at Unzen volcano. Dissertation

Cichy SB, Botcharnikov RE, Holtz F, Behrens H (2011) Vesiculation and microlite crystallization induced by decompression: a case study of the 1991–1995 Mt Unzen Eruption (Japan). J Petrol 52(7/8):1469–1492. https://doi.org/10.1093/petrology/egq072

Crank J (1975) The mathematics of diffusion. J Am Chem Soc. https://doi.org/10.1021/ja01562a070

Cunningham GJ, Henderson P, Lowry RK, Nolan J, Reed S, Long JV (1983) Lithium diffusion in silicate melts. Earth Planet Sci Lett 65:203–205. https://doi.org/10.1016/0012-821X(83)90199-1

De Hoog JCM (2018) Matrix effects during SIMS measurements of the lithium mass fractions of silicate glasses: correction procedures and updated preferred values of reference materials. Geostand Geoanalytical Res 42–4:513–522. https://doi.org/10.1111/ggr.12237

Dell WJ, Bray PJ, Xiao SZ (1983) 11B NMR studies and structural modelling of Na_2O-B_2O_3-SiO_2 glasses of high soda content. J Non-Cryst Solids 58:1–16. https://doi.org/10.1016/0022-3093(83)90097-2

Denny A, Zimmer MM, Cunningham HS (2021) Lithium isotope bias during SIMS analysis of silicate glass standards. Geol Soc Am Bull. https://doi.org/10.1130/abs/2021AM-371308

Dingwell DB, Pichavant M, Holtz F. (2002) Experimental studies of boron in granitic melts. In: Grew ES, Anovitz LM (eds). Boron mineralogy, petrology and geochemistry. In: Anovitz LM, Grew ES (eds). De Gruyter: Berlin, Boston 2018, p 331-386

Edmonds M, Wallace PJ (2017) Volatiles and exsolved vapor in volcanic systems. Elements 13:29–34. https://doi.org/10.2113/gselements.13.1.29

Giordano D, Russell JK, Dingwell DD (2008) Viscosity of magmatic liquids: a model. Earth Planet Sci Lett 271:123–134. https://doi.org/10.1016/j.epsl.2008.03.038

Gonnermann HM, Manga M (2007) The fluid mechanics inside a volcano. Annu Rev Fluid Mech 39:321–356. https://doi.org/10.1146/annurev.fluid.39.050905.110207

Hervig RL, Moore GM, Williams LB, Peacock SM, Holloway JR, Roggensack K (2002) Isotopic and elemental partitioning of boron between hydrous fluid and silicate melt. Amer Miner 87:769–774. https://doi.org/10.2138/am-2002-5-620

Hoefs J (2009) Stable isotope. Geochemistry. https://doi.org/10.1007/978-3-540-70708-0

Holycross ME, Watson EB, Richter FM, Villeneuve J (2018) Diffusive fractionation of Li isotopes in wet, highly silicic melts. Geochem Perspect Lett 6:39–42. https://doi.org/10.7185/geochemlet.1807

Huppert HE, Woods AW (2002) The role of volatiles in magma chamber dynamics. Lett Nat 420:493–495. https://doi.org/10.1038/nature01211

Hurwitz S, Navon O (1994) Bubble nucleation in rhyolitic melts: experiments at high pressure, temperature, and water content. Earth Planet Sci Lett 122:267–280. https://doi.org/10.1016/0012-821X(94)90001-9

Jambon A, Semet MP (1978) Lithium diffusion in silicate glasses of albite, orthoclase, and obsidian composition: an ion-microprobe

determination. Earth Planet Sci Lett 37:445–450. https://doi.org/10.1016/0012-821X(78)90060-2
Jochum PK, Weis U, Stoll B, Kuzmin D, Yang Q, Raczek I, Jacob DE, Stracke A, Birbaum K, Frick DA, Günther D, Enzweiler J (2011) Determination of reference values for NIST SRM 610–617 glasses following ISO guidelines. Geostand Geoanalytical Res 35(4):397–429. https://doi.org/10.1111/j.1751-908X.2011.00120.x
Kakihana H, Kotaka M, Satoh S, Nomura M, Okamoto M (1977) Fundamental studies on the Ion. exchange of boron isotopes. Bull Chem Soc Jpn 50:158–163. https://doi.org/10.1246/bcsj.50.158
Kargl F, Meyer A, Koza MM, Schober H (2006) Formation of channels for fast ion diffusion in alkali silicate melts: a quasielastic neutron scattering study. Phys Rev 74:014304. https://doi.org/10.1103/PhysRevB.74.014304
Le Losq C, Mysen BO, Cody GD (2015) Water and magmas: insights about the water solution mechanisms in alkali silicate melts from infrared, Raman and ^{29}Si solid-state NMR spectroscopies. Prog Earth Planet Sci 2:22. https://doi.org/10.1186/s40645-015-0052-7
Lee C, Lee SK (2020) Network polymerization and cation coordination environments in boron-bearing rhyolitic melts: insights from 17O, 11B and 27Al solid state NMR of sodium aluminoborosilicate glasses with varying boron content. Geochim Cosmochim Acta 268:325–347. https://doi.org/10.1016/j.gca.2019.10.010
Leeman WP, Sisson VB (2018) Geochemistry of boron and its implications for crustal and mantle processes. In: Anovitz LM, Grew ES (eds) Boron mineralogy, petrology, and geochemistry. De Gruyter, Berlin, Boston, pp 645–708. https://doi.org/10.1515/9781501509223-014
Lesher CE, Spera FJ (2015) Thermodynamic and transport properties of silicate melts and magma. In: Sigurdsson H (ed) The encyclopedia of volcanoes 113–141. Academic Press, Cambridge. https://doi.org/10.1016/B978-0-12-385938-9.00005-5
Marschall HR, Wanless VD, Shimizu N, Pogge von Strandmann PA, Elliott T, Monteleone BD (2017) The boron and lithium isotopic composition of mid-ocean ridge basalts and the mantle. Geochim Cosmochim Acta 207:102–138. https://doi.org/10.1016/j.gca.2017.03.028
Mills KC, Hayashi M, Wang L, Watanabe T. (2014) The structure and properties of silicate slags. In: Seetharaman S (ed). Treatise on process metallurgy, process fundamentals. p 149–286 https://doi.org/10.1016/C2010-0-66691-0
Mungall JE (2002) Empirical models relating viscosity and tracer diffusion in magmatic silicate melts. Geochim Cosmochim Acta 66(1):125–143. https://doi.org/10.1016/S0016-7037(01)00736-0
Mungall JE, Dingwell DB, Chaussidon M (1999) Chemical diffusivities of 18 trace elements in granitoid melts. Geochim Cosmochim Acta 63(17):2599–2610. https://doi.org/10.1016/S0016-7037(99)00209-4
Mysen B, Richet P (eds) (2018) Silicate glasses and melts, 2nd edn. Elsevier, Amsterdam, pp 411–460. https://doi.org/10.1016/B978-0-444-63708-6.09994-4
Pappalardo L, Buono G, Fanara S, Petrosino P (2018) Combining textural and geochemical investigations to explore the dynamics of magma ascent during plinian eruptions: a somma-vesuvius volcano (Italy) case study. Contrib Miner Pet 173:61. https://doi.org/10.1007/s00410-018-1486-x
Paton C, Hellstrom J, Paul B, Woodhead J, Hergt J (2011) Iolite: freeware for the visualisation and processing of mass spectrometric data. J Anal at Spectrom 26:2508. https://doi.org/10.1039/c1ja10172b
Penniston-Dorland S, Liu X-M, Rudnick RL (2017) 6 Lithium isotope geochemistry. In: Fang-Zhen T, James W, Nicolas D (eds) Non-traditional stable isotopes. De Gruyter, Berlin, Boston, pp 165–218. https://doi.org/10.1515/9783110545630-007
Pfennig G, Klewe-Nebenius H, Seelman-Eggebert W (1998) Chart of the nuclides, 6th edn. Forschungszentrum Karlsruhe GmbH, Karlsruhe, Germany
Richter FM, Liang Y, Davis AD (1999) Isotope fractionation by diffusion in molten oxides. Geochim Cosmochim Acta 63(18):2853–2861. https://doi.org/10.1016/S0016-7037(99)00164-7
Richter FM, Davis AM, DePaolo DJ, Watson B (2003) Isotope fractionation by chemical diffusion between molten basalt and rhyolite. Geochim Cosmochim Acta 67(20):3905–3923. https://doi.org/10.1016/S0016-7037(03)00174-1
Romer RR, Meixner A, Förster H-J (2014) Lithium and boron in late-orogenic granites—isotopic fingerprints for the source of crustal melts? Geochim Cosmochim Acta 131:98–114. https://doi.org/10.1016/j.gca.2014.01.018
Ross S, Welsch A-M, Behrens H (2015) Lithium conductivity in glasses of the Li_2O-Al_2O_3-SiO_2 system. Phys Chem Chem Phys 17:465–474. https://doi.org/10.1039/C4CP03609C
Rutherford MJ (2008) Magma ascent rates. Rev Miner Geochem 69:241–271. https://doi.org/10.2138/rmg.2008.69.7
Schiavi F, Bolfan-Casanova N, Withers AC, Médard E, Laumonier M, Laporte D, Flaherty T, Gómez-Ulla A (2018) Water quantification in silicate glasses by raman spectroscopy: correcting for the effects of confocality, density and ferric ion. Chem Geol 483:312–331. https://doi.org/10.1016/j.chemgeo.2018.02.036
Schmidt BC, Zotov N, Dupree R (2004) Structural implications of water and boron dissolution in albite glass. J Non-Cryst Solids 337:207–219. https://doi.org/10.1016/j.jnoncrysol.2004.04.007
Schulze F, Behrens H, Holtz F, Roux J, Johannes W (1996) The influence of H_2O on the viscosity of a haplogranitic melt. Amer Miner 81:1155–1165. https://doi.org/10.2138/am-1996-9-1014
Shewmon P (2016) Diffusion in solids. Springer, New york. https://doi.org/10.1007/978-3-319-48206-4
Stanton TR (1990) High-pressure, isotopic studies of the water diffusion mechanism in silicate melts and glasses. Arizona State University, Dissertation
Stolper E (1989) Temperature dependence of the speciation of water in rhyolitic melts and glasses. Am Miner 74(11–12):1247–1257
Tomascak PB, Magna T, Dohmen R (2016) Advances in lithium isotope geochemistry. In: Hrsg JH (ed) Springer. New York. https://doi.org/10.1007/978-3-319-01430-2
Toramaru A (2006) BND (bubble number density) decompression rate meter for explosive volcanic eruptions. J Volcanol Geotherm Res 154(3–4):303–316. https://doi.org/10.1016/j.jvolgeores.2006.03.027
Watkins JM, DePaolo DJ, Huber C, Ryerson FJ (2009) Liquid composition-dependence of calcium isotope fractionation during diffusion in molten silicates. Geochim Cosmochim Acta 73:7341–7359. https://doi.org/10.1016/j.gca.2009.09.004
Watkins JM, DePaolo DJ, Watson BE (2017) Kinetic fractionation of non-traditional stable isotopes by diffusion and crystal growth reactions. Rev Mineral Geochem 82:85–125. https://doi.org/10.2138/rmg.2017.82.4
Watson BE (2017) Diffusive fractionation of volatiles and their isotopes during bubble growth in magmas. Contrib Miner Pet 172:61. https://doi.org/10.1007/s00410-017-1384-7
Woodhead JD, Hellstrom J, Hergt JM, Greig A, Maas R (2007) Isotopic and elemental imaging of geological materials by laser ablation inductively coupled plasma-mass spectrometry. Geostand Geoanalytical Res 31(4):331–343. https://doi.org/10.1111/j.1751-908X.2007.00104.x
Wunder B, Mieixner A, Romer RL, Jahn S (2011) Li-isotope fractionation between silicates and fluids: pressure dependence and influence of the bonding environment. Eur J Mineral 23:333–342. https://doi.org/10.1127/0935-1221/2011/0023-2095

Xiang L, Romer RL, Glodny J, Trumbull RB, Wang R (2020) Li and B isotopic fractionation at the magmatic-hydrothermal transition of highly evolved granites. Lithos 376–377:105753. https://doi.org/10.1016/j.lithos.2020.105753

Zhang Y, Ni H, Chen Y (2010) Diffusion data in silicate melts. Rev Miner Geochem 72:311–408. https://doi.org/10.2138/rmg.2010.72.8

Zotov N, Yanev Y, Epelbaum M, Kostantinov L (1992) Effect of water on the structure of rhyolite glasses–X-ray diffraction and Raman spectroscopy studies. J Non-Cryst Solids 142:234–246. https://doi.org/10.1016/S0022-3093(05)80030-4